Local structure of $L1_2$-ordered $Ni_{75}(Al_{1-x}Fe_x)_{25}$ alloys

S. Pascarelli
Istituto Nazionale di Fisica Nucleare, Laboratori Nazionali di Frascati, CP-13, 00044 Frascati, (Rome), Italy and Consorzio Interuniversitario Nazionale Fisica della Materia, Via Dodecaneso 33, 16146 Genova, Italy

F. Boscherini
Istituto Nazionale di Fisica Nucleare, Laboratori Nazionali di Frascati, CP-13, 00044 Frascati, (Rome), Italy

S. Mobilio
Istituto Nazionale di Fisica Nucleare, Laboratori Nazionali di Frascati, CP-13, 00044 Frascati, (Rome), Italy and Dipartimento di Energetica, Università dell'Aquila, Roio Monteluco, L'Aquila, Italy

K. Lawniczak-Jablonska
Institute of Physics, Polish Academy of Sciences Al. Lotnikow 32/46, 02-668 Warszawa, Poland

R. Kozubski
Institute of Physics, Jagellonian University, Reymonta 4, 30-059 Krakow, Poland
(Received 10 August 1993; revised manuscript received 6 January 1994)

We present an Fe and Ni K-edge extended x-ray-absorption fine structure study of the $L1_2$-ordered ternary alloy $Ni_{75}(Al_{1-x}Fe_x)_{25}$. We find that Fe enters predominantly the Al sublattice of Ni_3Al (γ' phase). The distribution of Fe and Al atoms on this sublattice follows the expected distribution for an $L1_2$ structure. The Fe nearest-neighbor distances are consistent with the measured lattice parameters. The first coordination shell around Ni is composed of Ni, Fe, and Al atoms. The Ni-Ni and Ni-Fe bond lengths are consistent with diffraction data. On the other hand, an unexpected strong (≈ 0.2 Å) decrease of the Ni-Al distance with increasing Fe content is detected, the Ni-Al bond being also characterized by a large disorder. This result provides a local structural explanation to the large lattice strains recently measured in similar samples by x-ray diffraction.

I. INTRODUCTION

Ni_3Al is an intermetallic compound with an $L1_2$-type (γ' phase) structure. This lattice has a face-centered-cubic cell where face centers are occupied by Ni atoms, while Al atoms occupy cell corners, thus forming two separate sublattices.

Ni_3Al has very attractive high-temperature properties among which a positive temperature dependence of yield stress.[1] In recent years it has been proved that the mechanical properties of ordered binary $L1_2$ alloys are strongly modified by the addition of a third element.[1,2] In particular it was found that strength and ductility depend on the site preference and size misfit of the ternary element, because the local strain introduced in the lattice acts as a barrier against dislocation motion, resulting in the strengthening of the compound (solid-solution hardening).

In particular, several studies on Ni_3Al have shown that it can accommodate considerable amounts of ternary additions in solution, resulting in significant strengthening.[3–6] An x-ray-diffraction investigation of the local static strain in alloyed Ni_3Al showed that it depended largely on the nature of the alloying element.[7] The authors found an inverse correlation between the magnitude of strain in the Ni and Al sublattices in the presence of an alloying element (i.e., strain in one is large while in the other it is small).

As for the site preference, several different theoretical approaches have been used to model the substitutional behavior of ternary additions.[8–13] The theory of ternary site preference in Ni_3Al was developed by Guard and Westbrook.[8] These authors suggested that the substitutional behavior is not controlled by size effects but by the electronic structure of the ternary addition. Much later Morinaga, Yukawa, and Adachi studied the effect of Ni_3Al alloying on its electronic structure.[10] The authors found a correlation between the substitutional behavior and the resemblance of the profile in the density of states of the elemental additions to that of either Al or Ni. Furthermore, Freeman, Hong, and Xu, in a study of the structural phase stability of Ni_3Al with and without V additions,[11] related site preference to the position of the Fermi level with respect to the bonding and antibonding parts of the density of states, originating from the strong hybridization between the addition and the host.

It is now generally accepted that substitutional behavior is governed by alloy composition, temperature and relative magnitude of the effective-pair interactions (in our case the Ni-X and Al-X pair interactions). The substitutional behavior of a series of elements was recently predicted using the tetrahedron approximation of the

cluster variation method[12] and the phenomenological Lennard-Jones pair potential.[13] Based on this, alloying elements may be classified according to three types of site preference behavior: those which enter preferentially the Ni sublattice (Co and Cu), those which almost entirely substitute Al (Ti, Nb, Mo, Hf, Ta, and W), and finally those for which the substitution site strongly depends on composition and changes in passing through stoichiometry (Cr, Mn). Alloying atoms enter preferentially the Al sublattice in the case that the sum of the two concentrations is less than the stoichiometric composition (25 at. %), and they begin to enter the Ni sublattice only as the sum exceeds it.

Fe seems to belong to this last category of elements. The addition of Fe to Ni_3Al is particularly interesting also because it adds intriguing magnetic properties to the alloy, the behavior of which changes from paramagnetic to strongly ferromagnetic: alloys with $x \geq 0.2$ are ferromagnets at room temperature.[14] Besides the giant magnetic moments observed at very low Fe concentrations ($\ll 1\%$),[15,16] the mean atomic magnetic moment of the alloy increases from 0.08 to $1.2\mu_B$ in passing from Ni_3Al to Ni_3Fe.[17]

The Ni_3Al-Ni_3Fe diagram has been obtained by means of optical microscopy, x-ray-diffraction, and EPMA measurements of diffusion layers.[18] At low temperatures, $Ni_{75}(Al_{1-x}Fe_x)_{25}$ forms a continuous $L1_2$ solid solution (γ' phase); as the temperature increases a second phase, the disordered fcc (γ) phase, appears to be stable along with the γ', starting on the Fe-rich side at approximately 800 K, and then developing along the whole concentration range as temperature increases up to 1600 K for the Al-rich side. At intermediate temperatures therefore there is a two phase region ($\gamma+\gamma'$). Finally, as temperature increases further, the ordered γ' phase disappears.

The order-disorder transition temperature in the $Ni_{75}(Al_{1-x}Fe_x)_{25}$ system is a rapidly decreasing function of x.[18,19] This has been exploited to study long-range ordering kinetics as a function of ordering energies in quasibinary alloys $Ni_{75}(Al_{1-x}M_x)_{25}$ where M = Fe, Mn, Cr. The addition of M strongly affects γ' stability by controlling parameters related to long-range ordering kinetics in these systems. These effects have been the subject of intensive investigations,[20–22] and the strong demand for the precise knowledge of atomic configurations in these alloys gave rise to the present study.

There is still much controversy on the substitutional behavior of Fe in γ' Ni_3Al.[21–28] Mössbauer measurements indicate that site occupation is Fe concentration dependent.[24] The fraction of Fe atoms substituting Al sites was found to be 78% and 54% in alloys containing 2.5 at. % and 9.3 at. % Fe, respectively. On the other hand channeling enhanced microanalysis showed that this fraction depends on Ni content.[26] Three different compositions with a constant 5 at. % Fe content were investigated. The authors found that the fraction of Fe atoms substituting Al in $Ni_{70}Al_{25}Fe_5$, $Ni_{72.5}Al_{22.5}Fe_5$, and $Ni_{75}Al_{20}Fe_5$ was 30, 58, and 77 %, respectively.

Knowledge of the local structure of the $Ni_{75}(Al_{1-x}Fe_x)_{25}$ solid solution is fundamental to understanding its physical and chemical properties. The number and type of atoms surrounding Fe atoms allow to quantitatively establish Fe site preference; interatomic distances give insight into magnetic forces and solid solution strengthening, and are used to determine pair potentials, to predict phase stability and to compare directly to theoretical predictions.

Extended x-ray-absorption fine structure (EXAFS) is an ideal tool to investigate local atomic environment in alloys.[29,30] The possibility of "tuning in" to a particular absorption edge and thus studying local bonding properties (bond distances, coordination numbers, and atomic mean-square relative displacements) around each particular chemical species in an alloy is a specific advantage of this technique.

In the next section we describe sample preparation and the experimental setup and in Sec. III we briefly illustrate the data analysis method followed. In Secs. IV and V we list the results of the analysis for Fe and Ni K-edge data respectively. Finally, on the basis of the structural information obtained, the local structure of the alloy is described and discussed in Sec. VI.

II. EXPERIMENTAL

The $Ni_{75}(Al_{1-x}Fe_x)_{25}$ samples, with x = 0.0, 0.08, 0.20, 0.39, 0.55, and 1.0, were produced from 5N Al, 4N Ni, and 4N Fe. The alloys were cast in a high-frequency furnace under Ar flow and rapidly solidified. The samples were then annealed for one week at a temperature T_A below the corresponding γ' phase boundary, in order to obtain a maximum γ' homogeneity and large antiphase ordered domains. Samples No. 3 and 4 however were first homogenized above the γ' phase boundary as the corresponding T_A were too low to eliminate casting defects.[31] Homogeneity, effective composition and microstructure were tested by x-ray diffraction, scanning electron microscopy, and TEM. A homogeneous $L1_2$ superstructure with no antiphase boundaries was found in samples with low Fe content. At high Fe content $L1_2$ ordered domains (1000–5000 Å in diameter) were found to be separated by regions ($\approx$100 Å thick) containing smaller $L1_2$ ordered domains dispersed in a disordered matrix. The volume fraction of this disordered phase is of the order of a few percent of the total volume and thus does not affect the results.

The x-ray-diffraction measurements reported in Table I, show that as Fe content increases the lattice parameter decreases, in agreement with literature data.[18] The average distance $\langle d \rangle = a_0/\sqrt{2}$ between nearest neighbors, as predicted from the diffraction data of the alloys with $0 < x < 0.55$, varies between 2.523 and 2.517 Å, a variation which is too small to detect with the normal EXAFS accuracy of ± 0.01 Å.

As prepared samples, in the form of flat 1-mm-thick tablets, were used for fluorescence measurements. For x-ray absorption in the transmission mode the tablets were grated isolating the finest grains. To optimize sample homogeneity, the appropriate amount of sample was mixed to BN powder and pressed to form compact pellets.

EXAFS measurements were performed at the Labora-

TABLE I. Sample characteristics. The second column contains Fe concentration x in the $Ni_{75}(Al_{1-x}Fe_x)_{25}$ alloys. The third–sixth columns contain at. % of Fe, Al, Ni, and other elements, respectively. The seventh column contains lattice parameters as measured by x-ray diffraction.

Sample No.	x	at. % Fe	at. % Al	at. % Ni	at. % other	a_0 (Å)
0	0.00	0.0	24.0	75.0	1 (B)	3.5675±0.0005
1	0.08	2.1	22.6	75.3		3.5660±0.0005
2	0.20	4.9	19.3	75.8		3.5640±0.0005
3	0.39	9.7	14.2	76.1		3.5608±0.0005
4	0.55	13.8	9.4	76.8		3.5594±0.0005
5	1.00	25.0	0.0	75.0		

tori Nazionali di Frascati PULS synchrotron radiation facility, using the emission of the Adone storage ring during dedicated beam time; the storage ring was operated at 1.5 GeV and the average current was approximately 40 mA. The x-ray radiation was monochromatized using a Si(111) channel-cut crystal. The energy resolution at the Fe and Ni K-edge was between 3 and 4 eV. These values are slightly larger than the energy spread due to the finite lifetime of the core hole (Fe K, 1.0 eV, Ni K, 1.2 eV).[32] The harmonic content of the beam is negligible because of the low critical energy of the source (1.5 keV) and the absence of the $n=2$ reflection for Si(111).

Fe K-edge EXAFS was measured in the fluorescence mode at $T=77$ K (except sample No. 3) and at room temperature. The incoming beam intensity was measured by an ion chamber, while fluorescence photons were detected using a NaI(Tl) scintillator. A Mn filter was placed in front of the scintillator window in order to reduce the elastic-scattering background.

Ni K-edge data were recorded in the transmission mode at $T=77$ K. The x-ray absorption was measured by simultaneously recording the current from two ion chambers, one placed upstream and the other downstream from the sample.

III. DATA ANALYSIS

The absorption spectra were analyzed according to standard procedures.[33] The oscillating contribution was isolated from the total absorption coefficient by removing the pre-edge absorption and the atomic absorption above the edge. The former was fitted with a linear function while the latter with a spline curve. In a first approximation the threshold energy E_0 was fixed at the maximum slope energy. It was treated as an adjustable parameter in the further analysis. The normalized EXAFS oscillations, $\chi(k)$, relative to the low-temperature fluorescence data (corrected for reabsorption) at the Fe K-edge are reported in Fig. 1. In Fig. 2 we show the $\chi(k)$ functions relative to the Ni K-edge.

The EXAFS were multiplied by k^2 and Fourier transformed in order to separate the contributions from the various shells. A Hanning window was used in the range $k=2.5$–12.4 Å^{-1} and $k=2.1$–12.9 Å^{-1} for Fe and Ni K-edge data, respectively. The magnitudes of the Fourier transforms show peaks from at least four coordination shells. In Fig. 3 we show Ni K-edge data.

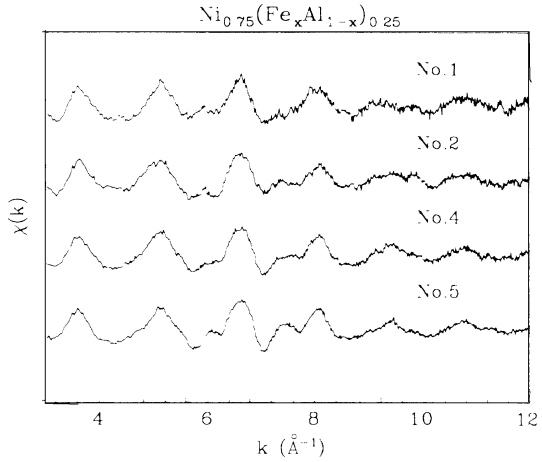

FIG. 1. Fe K-edge EXAFS measured in the fluorescence mode at $T=77$ K. Data as been corrected for reabsorption.

The first shell contribution was separated from the others by Fourier filtering a portion of R space back to k space. The R-space window was chosen to be from 1.7 to 2.7 Å and from 1.2 to 3.0 Å for the Fe and Ni K-edge data, respectively.

Quantitative data analysis was performed in k space. The filtered signal was fitted to a model signal using a least squares minimization routine. The definition of the minimized function is according to Ref. 34.

To obtain structural information on each type of bond belonging to the first shell, the $k\chi(k)$ filtered signal was fitted with a linear combination of model EXAFS spectra, one for each possible neighbor. Theoretical backscattering amplitudes and total phase shifts are used in the standard EXAFS formula making provision for variation of interatomic distances (R), E_0 offsets, mean-square relative displacements (σ^2), coordination numbers (N) and a damping coefficient γ, which appears in the standard EXAFS formula in the term $\exp[-2R/\gamma k]$.

To obtain physically meaningful results the number of

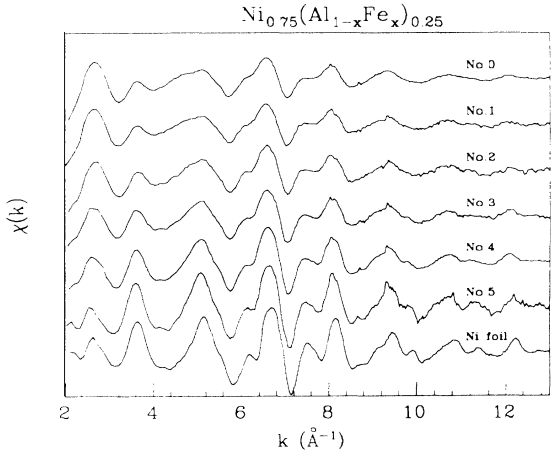

FIG. 2. Ni K-edge EXAFS measured in the transmission mode at $T=77$ K.

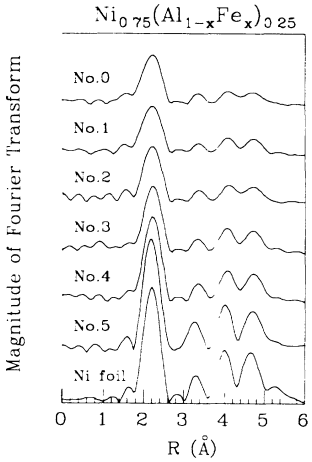

FIG. 3. Magnitude of Fourier transforms relative to Ni K-edge data.

independent parameters in the fitting routine was kept lower than the number of independent points $N_{\text{ind pts}}$ of the filtered signal.[34] The k-space interval used in the fitting procedure was equal to 4.5–12.0 Å^{-1} (yielding $N_{\text{ind pts}}=4.7$) and to 3.0–12.5 Å^{-1} (yielding $N_{\text{ind pts}}=10.8$) for Fe and Ni K-edge data, respectively.

In order to check the theoretical amplitudes and phases used[35,36] and estimate γ, we first of all fitted a spectrum relative to pure Ni measured in the same experimental conditions and analyzed using the same procedure. By fixing a coordination number of 12, we obtained $R_{\text{NiNi}}=2.483\pm0.008$ Å, $\sigma^2_{\text{NiNi}}=(4\pm1)\times10^{-3}$ Å^2, and $\gamma=1.7\pm0.3$ Å^2. The error bar on each parameter is obtained by changing that particular parameter until the value of the minimized function is doubled. The bond distance is equal to values found in literature, which vary between[37] 2.486 and[38] 2.492 Å, while the value of σ^2 obtained is consistent with a calculation[39] using the Debye approximation for the phonon density of states which gives $\sigma^2(77\text{ K})=3.1\times10^{-3}$ Å^2. Using the appropriate energy resolution and core-hole width the photoelectron inelastic mean free path is estimated to vary from $\lambda=15$ Å to $\lambda=60$ Å in the energy range between 35 and 550 eV, which compares well with values determined with other techniques.[40]

During least-squares minimization of the signals relative to the samples, due to the strong correlation between parameters, reliable coordination numbers, mean-square relative displacements, and damping factors could not be obtained without further assumptions. The damping coefficient γ was therefore fixed to the one found for pure Ni. The approximation lies in the fact that the photoelectron inelastic mean free path found for Ni is used for the intermetallic compounds.

IV. FE K-EDGE RESULTS

The data were corrected for reabsorption of fluorescence following Ref. 41. Using the concentration of the samples and the known x-ray-absorption coefficients we have estimated amplitude correction factors ranging from 0.95 to 0.62 and corrections to σ^2 smaller than 1×10^{-3} Å^2.

TABLE II. Best-fit structural parameters relative to Fe K-edge data. The second column contains the Fe concentration x in the $Ni_{75}(Al_{1-x}Fe_x)_{25}$ alloys. The third–fifth columns contain coordination numbers, interatomic distances, and mean-square relative displacements. The sixth column contains sample temperature during the EXAFS measurements.

Sample No.	x	N_{FeNi}	R_{FeNi} (Å)	σ^2_{FeNi} (10^{-3} Å^2)	T (K)
1	0.08	11±1	2.52±0.01	5±1	77
2	0.20	10±2	2.51±0.01	5±1	77
3	0.39	11±1	2.51±0.01	8±1	300
4	0.55	11±1	2.51±0.01	4±1	77
5	1.00	11±1	2.51±0.01	4±1	77

The fitting procedure started by introducing only an Fe-Ni contribution. The best fit structural parameters obtained are listed in Table II. We find that the Fe first shell signal can be described very well with only an Fe-Ni contribution.

The Fe-Ni bond distance is constant with composition and is equal to the average nearest-neighbor interatomic distance $\langle d \rangle$ obtained from the measured cell parameter a_0. The value obtained is consistent with a previous EXAFS Fe-Ni bond distance determination[37] in Ni_3Fe of 2.51 Å.

In order to understand Fe substitutional behavior it is important to check for the presence of Fe-Al or of Fe-Fe contributions in the first shell signal. Due to the backscattering behavior of Fe, Ni, and Al, it is much easier to isolate an Fe-Al contribution rather than an Fe-Fe one from a strong Fe-Ni background. When an Al contribution was added however, the fits (performed in the range 3.0–12.0 Å^{-1}) did not improve, indicating the absence of Al nearest neighbors, i.e., $N_{\text{FeAl}}=0$. This result is not surprising as it was quite evident, by simply looking at Fe K-edge raw data (Fig. 1), that the influence of Al on the Fe K-edge signal was absent or very weak. In fact, despite the different Al content in the samples, all spectra show similar features at low k values (where the influence of Al is strongest). However, due to the sensitivity of the technique, this measurement has quite a large error. We tried to give a quantitative estimate of the error in the following way. Increasing fixed values of N_{FeAl} were introduced in the fit until the minimized function doubled with respect to the minimum value found with only Ni nearest neighbors. In this way we estimated $\Delta N_{\text{FeAl}}=1$, i.e., a maximum of 1 Al atom in the first coordination shell around Fe.

V. NI K-EDGE RESULTS

Due to the similarity in Ni and Fe backscattering amplitudes and phases, EXAFS cannot distinguish Ni-Fe from Ni-Ni contributions. The first shell signal can therefore be described in terms of an average Ni-M contribution, due to Ni-Ni and Ni-Fe bonds ($N_{\text{Ni}M}=N_{\text{NiNi}}+N_{\text{NiFe}}$), and a Ni-Al contribution. The

best-fit structural parameters obtained were independent of the choice of using Ni or Fe backscattering functions in the theoretical Ni-M signal. The number of Fe near neighbors N_{NiFe} may then be obtained from $N_{\mathrm{Ni}M}$ assuming $N_{\mathrm{NiNi}}=8$, which reflects Ni first shell environment in a γ' ordered structure. We are justified in this assumption by the diffraction data and by the Fe K-edge results (see also the discussion). Once N_{NiFe} is known, structural parameters relative to the Ni-Ni bonds, R_{NiNi}, and σ^2_{NiNi}, are obtained from the following equations:

$$R_{\mathrm{NiNi}}=(N_{\mathrm{Ni}M}R_{\mathrm{Ni}M}-N_{\mathrm{NiFe}}R_{\mathrm{NiFe}})/N_{\mathrm{NiNi}} \quad (1)$$

and

$$\sigma^2_{\mathrm{NiNi}}=(N_{\mathrm{Ni}M}\sigma^2_{\mathrm{Ni}M}-N_{\mathrm{NiFe}}\sigma^2_{\mathrm{NiFe}})/N_{\mathrm{NiNi}} \quad (2)$$

where R_{NiFe} and σ^2_{NiFe} (equal to R_{FeNi} and σ^2_{FeNi}, respectively) are taken from Table II.

During minimization, due to strong correlation between parameters, reliable coordination numbers and mean-square relative displacements were obtained by fixing the total coordination number, $N_{\mathrm{Ni}M}+N_{\mathrm{NiAl}}$, equal to 12, which reflects Ni first shell environment in a γ' structure. This is a reasonable assumption on the base of diffraction data and Fe K-edge results. The best fit parameters are listed in Table III. An example of fit obtained is reported in Fig. 4.

We shall first discuss the results obtained in pure Ni_3Al. The Ni-Ni and Ni-Al interatomic distances are consistent with the measured lattice parameter. Nasu *et al.* in an EXAFS study of Ni_3Al prepared by arc melting report values for these quantities which are 0.04 Å less than ours.[42] We suggest that the different theoretical phases used might be at the origin of this discrepancy. As for mean square relative displacements, we find values of σ^2_{NiNi} and of σ^2_{NiAl} which are at least two and seven times larger, respectively, in our sample compared to those reported by Nasu *et al.* We suggest this difference is mainly due to the different sample preparation methods, arc melting yielding samples characterized by a higher structural order.

We shall now analyze the results obtained for the alloys. The average number of Fe nearest neighbors increases with Fe concentration, going from a minimum of 0.3 atoms to a maximum of 4.0 in Ni_3Fe. The Ni-Ni interatomic distance obtained from $R_{\mathrm{Ni}M}$ using (1) is found to be constant with composition throughout the concentration range $x=0.00$ to $x=0.55$ and equal to 2.51 ± 0.01 Å, the average value expected for an fcc structure with cell dimensions given by the measured a_0. In Ni_3Fe we find a Ni-Ni bond equal to 2.48 Å, the value found in pure Ni. The degree of disorder on the Ni-Ni bond, σ^2_{NiNi}, obtained from $\sigma^2_{\mathrm{Ni}M}$ using (2), is highest at low Fe content ($\sigma^2_{\mathrm{NiNi}}\approx 7\times10^{-3}$ Å^2), and decreases in passing from Ni_3Al to Ni_3Fe to the value found in pure Ni ($\sigma^2_{\mathrm{NiNi}}\approx 4\times10^{-3}$ Å^2). The Ni-Al interatomic distance decreases rapidly with increasing Fe content and is characterized by a large degree of disorder, the relative root-mean-square bond deviation ($\sqrt{\sigma^2}/R$) being about 5%.

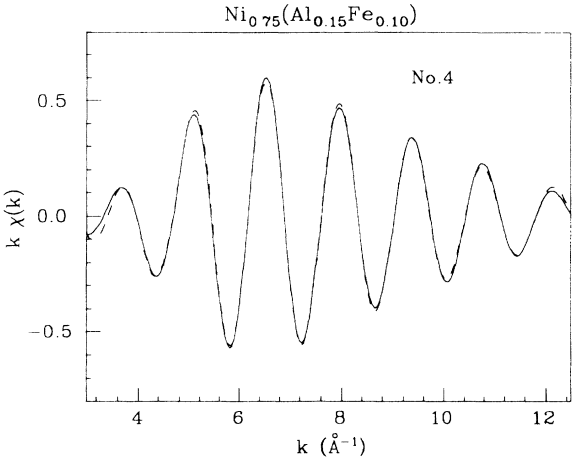

FIG. 4. Best fit to the filtered Ni K-edge EXAFS signal for sample No. 4. Average Ni-M (M =Ni,Fe) and Ni-Al contributions are included. We show the $k\chi(k)$ signal as the solid line and the fit as the dashed line.

VI. DISCUSSION

In Ni_3Al (γ' phase) two separate sublattices may be distinguished one formed by the face centers of the cubic cell and the other by the cell corners. The former is the "Ni sublattice" and the latter the "Al sublattice". If the

TABLE III. Best-fit structural parameters relative to Ni K-edge data. The second column contains the Fe concentration x in the $Ni_{75}(Al_{1-x}Fe_x)_{25}$ alloys. The third–fifth columns contain coordination numbers, interatomic distances and mean-square relative displacements relative to the average Ni-M (M=Ni,Fe) contribution. The sixth–eighth columns are relative to the Ni-Al contribution.

Sample No.	x	$N_{\mathrm{Ni}M}$	$R_{\mathrm{Ni}M}$ (Å)	$\sigma^2_{\mathrm{Ni}M}$ (10^{-3} Å^2)	N_{NiAl}	R_{NiAl} (Å)	σ^2_{NiAl} (10^{-3} Å^2)
0	0.00	8.0	2.51±0.01[a]	7±1	4.0±0.8	2.51[a]	15±5
1	0.08	8.3	2.51±0.01	6±1	3.7±0.5	2.50±0.04	15±5
2	0.20	8.8	2.51±0.01	5±1	3.2±1.0	2.43±0.09	20±10
3	0.39	9.6	2.51±0.01	5±1	2.4±0.6	2.37±0.08	20±10
4	0.55	10.4	2.51±0.01	4±1	1.6±0.6	2.32±0.06	12±5
5	1.00	12.0	2.49±0.01	4±1			

[a]Parameters set equal in the minimization procedure.

admixed Fe atoms were to enter exclusively the Al sublattice the first coordination shell of Fe would be composed of 12 Ni atoms. On the other hand, the first shell of the Ni atoms would be composed of eight Ni atoms and a total of four among Fe and Al atoms.

If Fe atoms were to enter also the Ni sublattice, a more complex situation would arise: the first shell of Fe would be composed of Ni, Fe, and Al. As long as a difference in site occupation probabilities of Ni and Al on the two sublattices is present a γ' superstructure would still be observed, however, it would become harder to distinguish the two sublattices. If Fe were to substitute randomly for both Ni and Al, in the limit of $x=1$ the structure would be composed of Ni and Fe atoms distributed randomly on a single average fcc lattice (the γ phase). In this situation the composition of the first coordination shell would be determined uniquely by atomic concentrations: $N_{NiNi}=N_{FeNi}=9$; $N_{NiFe}=N_{FeFe}=3$.

From Fe K-edge data we estimate that at most 1 nearest neighbor of Fe is Al, the rest being Ni; however the best fit is found for no Al nearest neighbors. These results are consistent with a γ' structure in which most of the Fe atoms (over 75% of the total) enter the Al sublattice, in agreement with the diffraction data and with Ref. 26. The Fe-Ni bond length is also found to be in agreement with diffraction data, for all the samples for which this data is available.

The EXAFS results at the Ni K-edge, listed in Table III, show that Ni is surrounded by a total of N_{NiM} among Ni and Fe atoms and by N_{NiAl}Al atoms. Once total contributions $N_{NiM}+N_{NiAl}$ and N_{NiNi} are fixed, there is a single free coordination parameter: N_{NiFe}/N_{NiAl}. In all samples, the best fit is obtained when this ratio reflects average γ' environment around Ni, as can be seen in Fig. 5, where best fit values are compared with the expected N_{NiFe}/N_{NiAl} values in an $L1_2$ ordered structure (dashed line). The Ni-Ni bond distance is constant and equal to 2.51 ± 0.01 Å throughout the composition range $0<x<0.55$, consistent with the measured lattice parameter.

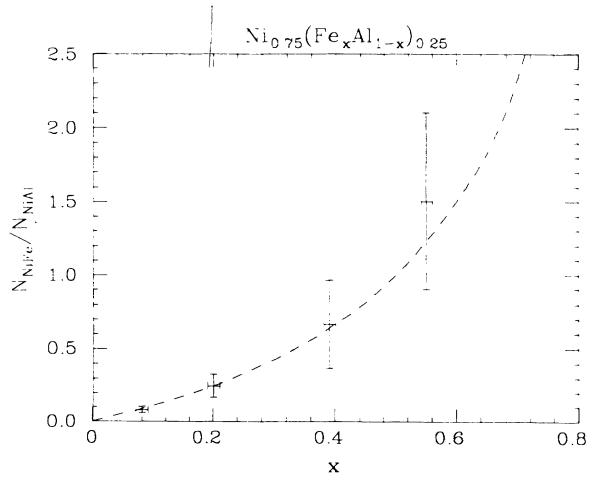

FIG. 5. The dashed curve indicates the ratio N_{NiFe}/N_{NiAl} in an $L1_2$ structure. Values of N_{NiFe}/N_{NiAl} obtained from Ni K-edge data are shown to follow the expected distribution for the $L1_2$ phase.

On the other hand the Ni-Al bond distance detected decreases strongly with composition. The relative bond distortion $\delta R_{NiAl}/a_0$, where $\delta R_{NiAl}=\langle d\rangle - R_{NiAl}$, increases with Fe content, reaching a maximum of 8% in sample No. 4. The structure in the presence of such "short" Ni-Al bonds can be explained in terms of distortions which involve either sublattice, or both. If the Ni sublattice were to sustain all of the distortion (the Ni atoms surrounding an Al atom moving closer to it), only "short" Ni-Al bonds would be present, but there would have to be several different Ni-Ni bond distances, which have not been detected. In the case of distortion of the Al sublattice only (the Al atom moves with respect to the Ni sublattice), the presence of "short" Ni-Al bonds would have to be accompanied by "normal" and "long" bonds as well. On the basis of the analysis we cannot exclude the presence of Ni-Al contributions at distances other than the one detected. In fact no more than one Ni-Al contribution can be included in the fit due to the limit on the maximum number of free parameters.

In the presence of three separate Ni-Al contributions it is not surprising that this data analysis is most sensitive to the one corresponding to the shortest distance, as the signal due to the "normal" bonds would lie at the same frequency of the strong Ni-M contribution, and the "long" bonds would be of the order of 40% less intense due to the larger R. Therefore, we are not able to completely solve this structure, but, based on the detected Ni-Al bond length and on mean-square relative displacement values we may conclude that the position of the Al atoms in these alloys is displaced from the average sublattice sites, has large fluctuations (up to 6%) and is strongly composition dependent. It is the Ni-Al bond therefore that introduces strain in the Al sublattice, the magnitude of which increases with Fe content.

The strain on both Ni and Al sublattices has been measured[7] by x-ray diffraction in different $Ni_{75}Al_{20}X_5$ alloys, where X was chosen among several transition elements, including Fe. The authors find that there is a correlation between strain on the two sublattices, i.e., when strain is large on one sublattice it is small on the other and vice versa. In the $Ni_{75}Al_{20}Fe_5$ sample they find a low amount of strain on the Ni sublattice and a higher strain on the Al sublattice. They find ε(Al sublattice)=3.4% where ε is defined as the root-mean-square displacement per atom (as measured by x-ray diffraction) divided by the cell parameter.

This situation is consistent with our findings on the local structure of $Ni_{75}(Al_{1-x}Fe_x)_{25}$ alloys. In sample No. 2, which is similar to the one investigated by Morinaga *et al.*,[7] we find $\delta R_{NiAl}/a_0=2.5\%$. The present measurements yield a local structural explanation to the results of Morinaga *et al.* which were obtained by x-ray diffraction, a technique which inherently yields chemically and site averaged information.

Similar bond distortions have been recently found in the crystalline solid solution $Fe_{22.5}Ni_{77.5}$ (γ phase). In an anomalous diffraction study, the components of atomic pair displacements with respect to the average lattice sites were measured.[43] A large increase of the Fe-Fe distance in the [110] direction was found which could not be

explained by a hard-sphere model. The authors pointed to the possible magnetic origin of this unexpected finding.

The progressive displacement of the Al atoms with respect to the lattice sites as Fe is added to Ni_3Al could be related to the local changes in the electronic wave functions in the Al environment. In fact the influence of a number of transition elements on the electronic structure of Ni_3Al has been investigated using the *DV-Xα* cluster method.[10] The calculations show that when a transition element, *M*, is alloyed into Ni_3Al, new energy levels due to the *M d* orbitals appear above the Fermi level. The authors found that as *M* replaces Al around Ni, the covalency of the newly formed *M*-Ni bond increases due to the presence of an enhanced *d* orbital component of *M*. The present data suggest that a consequence of this change of the wave functions around Ni is a redistribution of charge in the remaining Ni-Al bonds as Fe substitution progresses, which leads to local distortions and bond length fluctuation.

Alloying with Fe also induces strong changes in the magnetic properties of Ni_3Al. A study on the magnetic properties of $Ni_{75}(Al_{1-x}Fe_x)_{25}$ alloys shows that there is an increment of the degree of magnetic polarization of the *d* band as Fe content increases.[17] The detected displacement of the Al atoms could in this sense be driven by forces of magnetic origin, the influence of which increases with Fe content.

ACKNOWLEDGMENT

The authors would like to thank V. Rosato (ENEA, Casaccia) for stimulating discussions.

[1]D. P. Pope and S. S. Ezz, Int. Metall. Rev. **29**, 136 (1984).
[2]T. Suzuki, Y. Oya, and D. M. Wee, Acta Metall. **28**, 301 (1980).
[3]R. D. Rawlings and A. E. Staton-Bevan, J. Mater. Sci. **10**, 505 (1975).
[4]C. T. Liu, C. L. White, and J. A. Horton, Acta Metall. **33**, 213 (1985).
[5]A. Inoue, H. Tomioka, and T. Masumoto, Metall. Trans. **14A**, 1367 (1983).
[6]T. Takasugi and O. Izumi, Acta Metall. **33**, 1259 (1985).
[7]M. Morinaga, K. Sone, T. Kamimura, K. Ohtaka, and N. Yukawa, J. Appl. Crystallogr. **21**, 41 (1988).
[8]R. W. Guard and J. H. Westbrook, Trans. Metall. Soc. AIME **215**, 807 (1959).
[9]S. Ochiai, Y. Oya, and T. Suzuki, Acta Metall. **32**, 289 (1984).
[10]M. Morinaga, N. Yukawa, and H. Adachi, J. Phys. Soc. Jpn. **53**, 653 (1984).
[11]A. J. Freeman, T. Hong, and J. H. Xu, in *Atomic Simulations of Materials (beyond pair potentials)*, edited by V. Vitek and D. J. Srolovitz (Plenum, New York, 1989), pp. 41.
[12]Y. P. Wu, N. C. Tso, J. M. Sanchez, and J. K. Tien, Acta Metall. **37**, 2835 (1989).
[13]M. Enomoto and H. Harada, Metall. Trans. A **20**, 649 (1989).
[14]K. G. Efthimiadis, J. G. Antonopoulos, and I. A. Tsoukalas, Solid State Commun. **70**, 903 (1989).
[15]F. R. De Boer, C. J. Shinkel, J. Biesterbos, and S. Proost, J. Appl. Phys. **40**, 1049 (1969).
[16]P. L. Ling and T. J. Hicks, J. Phys. F **3**, 697 (1973).
[17]K. G. Efthimiadis and I. A. Tsoukalas, Solid State Commun. **85**, 81 (1993).
[18]N. Masahashi, H. Kawazoe, T. Takasugi, and O. Izumi, Z. Metallkd. **78**, 788 (1987).
[19]R. W. Cahn, P. A. Siemers, J. E. Geiger, and P. Bardhan, Acta Metall. **35**, 2737 (1987).
[20]R. Kozubski, J. Soltys, and M. C. Cadeville, J. Phys. Condens. Matter **2**, 3451 (1990).
[21]R. Kozubski, J. Soltys, M. C. Cadeville, V. Pierron-Bohnes, T. H. Kim, P. Schwander, J. P. Hahn, G. Kostorz, and J. Morgiel, Intermetallics (to be published).
[22]B. L. Bramfitt and J. R. Michael, in *Materials Problem Solving with the Transmission Electron Microscope*, edited by L. W. Hobbs, K. W. Westmacott, and D. B. Williams, MRS Symposia Proceedings No. 62 (Materials Research Society, Pittsburgh, 1986), p. 201.
[23]J. W. Drijver and F. van der Woude, J. Phys. F **3**, L206 (1973).
[24]J. R. Nicholls and R. D. Rawlings, Acta Metall. **25**, 187 (1977).
[25]M. K. Miller and J. A. Horton, Scr. Metall. **20**, 1125 (1986).
[26]D. Shindo, M. Kikuchi, M. Hirabayashi, S. Hanada, and O. Izumi, Trans. Jpn. Inst. Met. **29**, 956 (1988).
[27]A. Chiba, D. Shindo, and S. Hanada, Acta Metall. Mater. **39**, 13 (1991).
[28]D. Blavette and S. Chambreland, J. Phys. Colloq. (Paris) **47**, C2-227 (1986).
[29]D. Sayers, E. Stern, and F. W. Lytle, Phys. Rev. Lett. **27**, 1204 (1971).
[30]P. A. Lee, P. H. Citrin, P. Eisenberger, and B. M. Kincaid, Rev. Mod. Phys. **53**, 769 (1981).
[31]R. Kozubski, J. Soltys, M. C. Cadeville, and V. Oierron-Bohnes, in *Kinetics of Phase Transformations*, edited by M. O. Thompson, M. J. Aziz, and G. B. Stephenson, MRS Symposia Proceedings No. 205 (Materials Research Society, Pittsburgh, 1992), p. 153.
[32]K. D. Sevier, in *Low Energy Electron Spectrometry* (Wiley-Interscience, Chichester, UK, 1972), Chap. 6, p. 220.
[33]B. Lengeler and P. Eisenberger, Phys. Rev. B **21**, 4507 (1980).
[34]F. W. Lytle, D. E. Sayers, and E. A. Stern, Physica B **158**, 701 (1989).
[35]B. K. Teo and P. A. Lee, J. Am. Chem. Soc. **101**, 2815 (1979).
[36]A. G. McKale, B. W. Veal, A. P. Paulikas, S. K. Chan, and G. S. Knapp, J. Am. Chem. Soc. **110**, 3763 (1988).
[37]U. Scheuer and B. Lengeler, Phys. Rev. B **44**, 9883 (1991).
[38]H. W. King, Bull. Alloy Phase Diagrams **2**, 401 (1981).
[39]E. D. Crozier, J. J. Rehr, and R. Ingalls, in *X-ray Absorption: Principles, Applications, Techniques of EXAFS, SEXAFS and XANES*, edited by D. C. Koningsberger and R. Prins (Wiley, New York, 1988), Chap. 9, p. 373.
[40]M. P. Seah and W. A. Dench, Surf. Interface Anal. **1**, 2 (1979).
[41]Z. Tan, J. I. Budnick, and S. M. Heald, Rev. Sci. Instrum. **60**, 1021 (1989).
[42]T. Nasu, C. C. Koch, A. M. Edwards, and D. E. Sayers, J. Non-Cryst. Solids **150**, 491 (1992).
[43]G. E. Ice, C. J. Sparks, A. Habenschuss, and L. B. Shaffer, Phys. Rev. Lett. **68**, 863 (1992).